Available online at www.sciencedirect.com
ScienceDirect
C. R. Physique 7 (2006) 650–669
COMPTES RENDUS PHYSIQUE
http://france.elsevier.com/direct/COMREN/

Turbulent transport in fusion magnetised plasmas/Transport turbulent dans les plasmas magnétisés de fusion

Kinetic simulations of turbulent fusion plasmas

Yasuhiro Idomura [a,*], Tomo-Hiko Watanabe [b], Hideo Sugama [b]

[a] *Japan Atomic Energy Agency, Higashi-Ueno 6-9-3, Taitou, Tokyo 110-0015, Japan*
[b] *National Institute for Fusion Science/The Graduate University for Advanced Studies, Toki, Gifu 509-5292, Japan*

Available online 22 August 2006

Abstract

In contrast to neutral fluid turbulence described in three-dimensional (3D) configuration space, collisionless magnetised plasma turbulence has been studied using the gyrokinetic model, which is a reduced kinetic model of a plasma in 5D phase space. Recent advances in computer technology and simulation models enabled a direct numerical simulation of plasma turbulence in a toroidal configuration with experimentally relevant parameters. Such kinetic simulations have been established as an essential tool for studying turbulent transport in a fusion plasma. This overview summarises progress in kinetic simulations of turbulent fusion plasmas focusing on physical and numerical models and physical findings obtained from 5D gyrokinetic simulations. ***To cite this article: Y. Idomura et al., C. R. Physique 7 (2006).***

Résumé

Simulations cinétiques de la turbulence dans les plasmas de fusion. La turbulence dans un plasma magnétisé faiblement collisionnel est décrite par un modèle gyrocinétique à 5 dimensions dans l'espace des phases, ce qui conduit à des différences notables avec la turbulence en dynamique des fluides neutres, qui est usuellement décrite dans un espace à 3 dimensions. Les progrès récents en matière de calculateurs et de méthodes numériques ont permis de réaliser des simulations directes de plasmas turbulents en géométrie toroidale dans des conditions réalistes. Ces outils numériques sont désormais essentiels pour étudier le transport turbulent dans les plasmas de fusion. Cette revue synthétise les progrès réalisés dans le domaine des simulations cinétiques de plasmas turbulents, avec un accent particulier sur les modèles numériques et les résultats de physique obtenus avec les modèles gyrocinétiques. ***Pour citer cet article : Y. Idomura et al., C. R. Physique 7 (2006).***

Keywords: Plasma fusion; Turbulent fusion plasmas

Mots-clés : Fusion de plasmas ; Turbulence dans les plasmas de fusion

1. Introduction

Turbulence is a common phenomenon observed in most fluids, and is characterised by its chaotic behaviour and turbulent mixing leading to much larger transport than the molecular diffusion. Such turbulent transport is often observed also in a fusion plasma. Although a theoretical model for the transport due to Coulomb collisions in a

* Corresponding author.
E-mail address: idomura.yasuhiro@jaea.go.jp (Y. Idomura).

1631-0705/$ – see front matter
doi:10.1016/j.crhy.2006.06.007

stable, quiescent toroidal plasma was successfully established with taking into account particle orbits in a toroidal magnetic configuration [1,2], the transport levels observed in the experiment normally exceeds predictions by this collisional transport model, and a dominating cause is considered as plasma turbulence driven by micro-instabilities, which are characterised by microscopic scale lengths typically given by the Larmor radius. Since the confinement performance is an important factor in determining the size and cost of a fusion reactor, understanding of plasma turbulence is one of critical issues in fusion science [3]. However, because of its basic properties such as large degrees of freedom, strong nonlinearity, and sensitivity to the initial condition, a theoretical treatment of turbulence is an extremely difficult issue, and even neutral fluid turbulence is still an formidable physical problem. In addition, plasma turbulence is an even more complex phenomenon because of the following features. Firstly, multiple fluids (an electron fluid and other ion fluids) with considerably different mobility are coupled through electromagnetic fields and weak collisional interactions. Secondly, strong confinement fields provide highly anisotropic turbulent structures. Thirdly, inhomogeneities in density, temperature, and magnetic fields excite multiple micro-instabilities over wide spectral ranges. In particular, a toroidal magnetic configuration strongly affects the linear properties of micro-instabilities as well as nonlinearly evolved turbulent structures. Finally, because of weak collisionality in a high temperature core plasma, which is often called collisionless, a particle distribution function is deviated from a local thermodynamic equilibrium. In addition, kinetic effects such as wave-particle resonant interactions and particle orbit effects play essential roles in collisionless plasma turbulence. Because of this collisionless character, conventional fluid models such as a magnetohydrodynamics (MHD) model becomes insufficient, and kinetic descriptions of a plasma in phase space are needed. As in a research of neutral fluid turbulence, theoretical treatments of plasma turbulence have been actively studied based on dimensional analysis techniques and renormalisation approaches using statistical theories, and their progress were discussed in recent reviews [4,5]. However, because of the complexity of the phenomena, they have not matured to cover a broad parameter range in the experiment. On the other hand, a direct numerical simulation (DNS) is becoming important not only as a complementary approach to obtain physical understanding but also as an essential tool for predicting turbulent spectrum and transport in the experiment [6]. In contrast to neutral fluid turbulence described in three-dimensional (3D) configuration space, a primitive kinetic model of plasma turbulence is given by using a particle distribution function in 6D phase space. Because of this huge requirement on computational resources, DNS of experimentally relevant plasma turbulence was prohibitive before developments of advanced simulation models and modern supercomputers. In particular, the gyrokinetic model simplified the problem from 6D to 5D and reduced a computational cost by making micro-turbulence simulations free from irrelevant high-frequency phenomena associated with particles' gyro-motion. In addition to the physical model, numerical methods have also been improved to simulate plasma turbulence efficiently using advanced Lagrangian and Eulerian schemes with field aligned coordinates. The rapid progress of computational power extremely enhanced the capabilities of gyrokinetic simulations, and DNS of tokamak micro-turbulence has been established as an essential tool for studying tokamak turbulent transport. Recent gyrokinetic simulations have provided qualitative understanding of rich physics behind tokamak turbulent transport as well as quantitative estimations for key engineering issues such as the plasma size scaling of turbulent transport.

While comprehensive historical review of gyrokinetic simulations was given, for example, in [6–9], this overview summarises recent progress in a gyrokinetic simulation focusing on following topics. Section 2 presents theoretical frameworks of physical models from the 6D Vlasov equation to the 5D gyrokinetic equation. Section 3 discusses properties of numerical approaches used in recent gyrokinetic simulations. Section 4 describes several important physical findings obtained from 5D gyrokinetic simulations. Finally, the present status and future directions are discussed in Section 5.

2. Physical model

2.1. Kinetic model

In principle, a plasma may be completely described by the Newton–Maxwell system or the Klimontovich–Maxwell system. However, a fusion plasma consists typically of $\sim 10^{20}$ m^{-3} of ions and electrons, and it is unrealistic to trace all of them even with present-day and foreseeable future computers. Therefore, instead of solving all the particle motion, a statistical approach is introduced to describe a plasma by a particle distribution function. In a high temperature fusion plasma with $\sim$10 keV, the kinetic energy is much larger than the average potential energy between particles,

which means that particles are weakly coupled with each other. In such a weakly coupled plasma, multiple particle correlations more than three particle interaction are neglected, and two particle interaction is reduced to a collision operator $C(f_s)$ for a single particle distribution function $f_s(\mathbf{q}, \mathbf{p})$ in six-dimensional (6D) phase space $\mathbf{Z}_{\mathrm{CC}} = (\mathbf{q}, \mathbf{p})$ [10], where $\mathbf{q}$ and $\mathbf{p}$ are the position and momentum of a particle, respectively. As a result, an evolution equation of f_s is given by the Boltzmann equation,

$$\frac{Df_s}{Dt} \equiv \frac{\partial f_s}{\partial t} + \{f_s, H_s\} = C(f_s) \tag{1}$$

where $\{\cdot, \cdot\}$ is the Poisson bracket in the canonical coordinates $(\mathbf{q}, \mathbf{p})$,

$$\{F, G\} = \frac{\partial F}{\partial q_i}\frac{\partial G}{\partial p_i} - \frac{\partial F}{\partial p_i}\frac{\partial G}{\partial q_i} \tag{2}$$

and $H_s(\mathbf{q}, \mathbf{p})$ is the Hamiltonian of collisionless single particle motion,

$$H_s(\mathbf{q}, \mathbf{p}) = \frac{1}{2m_s}\left|\mathbf{p} - \frac{e_s}{c}\mathbf{A}\right|^2 + e_s\phi \tag{3}$$

Here, e_s and m_s are the charge and mass of the particle species s, c is the velocity of light, ϕ is the electrostatic potential, and $\mathbf{A}$ is the vector potential for the magnetic field $\mathbf{B} = \nabla \times \mathbf{A}$. In considering micro-turbulence, a collisionless model is often used, because the collision frequency, ν_{ss}, is much lower than characteristic frequencies of turbulent fluctuations such as drift waves ω_s^* and kinetic Alfvèn waves v_A/a (see Fig. 1). In the collisionless limit with $C(f_s) = 0$, Eq. (1) yields the Vlasov equation or the collisionless Boltzmann equation,

$$\frac{Df_s}{Dt} \equiv \frac{\partial f_s}{\partial t} + \{f_s, H_s\} = 0 \tag{4}$$

By taking the velocity moments of f_s, the particle density n_s and the current density $\mathbf{j}_s$ in the configuration space $\mathbf{q}$ are obtained as

$$n_s = \int f_s \, \mathrm{d}^3 p \tag{5}$$

$$\mathbf{j}_s = e_s \int \mathbf{v} f_s \, \mathrm{d}^3 p \tag{6}$$

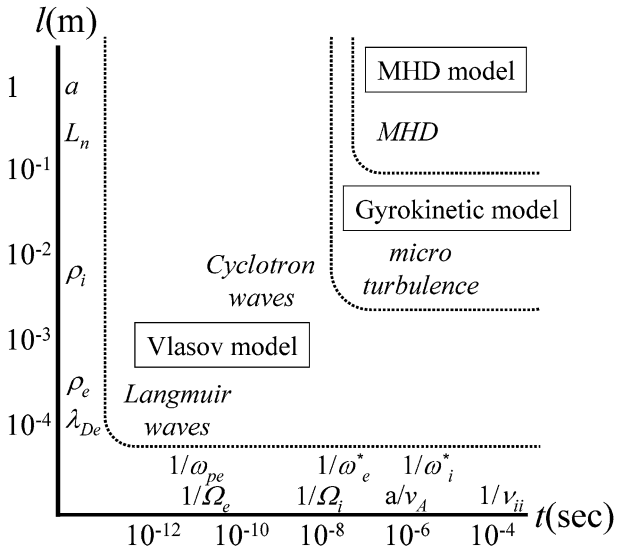

Fig. 1. Enormous ranges of spatio-temporal scales in a fusion plasma and applicability of Vlasov, gyrokinetic, and MHD models. Here, ω_{ps} is the plasma oscillation frequency, Ω_s is the Cyclotron frequency, ω_s^* is the diamagnetic rotation frequency, v_A is the Alfvèn velocity, ν_{ii} is the ion–ion collision frequency, λ_{Ds} is the Debye length, ρ_s is the Larmor radius, L_n is the scale length of the equilibrium density profile, a is the plasma size, and s denotes the particle species.

where $\mathbf{v} = [\mathbf{p} - (e_s/c)\mathbf{A}]/m_s$. The electromagnetic fields, $\mathbf{E}$ and $\mathbf{B}$, are determined by substituting n_s and $\mathbf{j}_s$ to the Maxwell equations,

$$\nabla \times \mathbf{E} = -\frac{1}{c}\frac{\partial \mathbf{B}}{\partial t} \tag{7}$$

$$\nabla \times \mathbf{B} = \frac{4\pi}{c}\sum_s \mathbf{j}_s + \frac{1}{c}\frac{\partial \mathbf{E}}{\partial t} \tag{8}$$

$$\nabla \cdot \mathbf{E} = 4\pi \sum_s e_s n_s \tag{9}$$

$$\nabla \cdot \mathbf{B} = 0 \tag{10}$$

The Vlasov–Maxwell system, Eqs. (4)–(10), gives the most fundamental description of a high temperature collisionless plasma.

2.2. Gyrokinetic model

Although the Vlasov–Maxwell system is a reduced kinetic description compared to the Newton–Maxwell system, it involves enormous ranges of spatio-temporal scales as shown in Fig. 1. Therefore, it is still prohibitive to simulate low frequency phenomena such as micro-turbulence and MHD waves via the Vlasov–Maxwell system. To avoid a direct treatment of multiple hierarchy spatio-temporal scales, a gyrokinetic model has been developed by eliminating high-frequency phenomena with $\omega > \Omega_s$ with keeping essential kinetic effects, where $\Omega_s = (e_s B_0)/(m_s c)$ is the Cyclotron frequency. While the earlier gyrokinetic equation was formulated by gyro-averaging the Vlasov equation based on the recursive method [11], the modern gyrokinetic theory [12–18] reviewed here has been developed based on the Hamiltonian or Lagrangian formalism with the Lie perturbation theory [19,20]. The latter approach enables rigorous treatments of the first principles such as the symmetry and the conservation properties, which are essential to describe underlying physics and useful for a nonlinear simulation.

From experimental observations, tokamak micro-turbulence is considered to obey the gyrokinetic ordering in a smallness parameter ε_g,

$$\frac{\omega}{\Omega_s} \sim \frac{k_\parallel}{k_\perp} \sim \frac{e_s\phi}{T_s} \sim \frac{B_1}{B_0} \sim \frac{\rho_s}{L_n} \sim \mathcal{O}(\varepsilon_g) \tag{11}$$

where ω is a characteristic frequency of micro-turbulence, $\mathbf{B}_0 = \nabla \times \mathbf{A}_0$ is the equilibrium field, $\mathbf{B}_1 = \nabla \times \mathbf{A}_1$ is the perturbed field, $\mathbf{b} = \mathbf{B}_0/B_0$ is the unit vector in the direction of $\mathbf{B}_0$, $k_\parallel = \mathbf{k}\cdot\mathbf{b}$ and $k_\perp = |\mathbf{k}\times\mathbf{b}|$ are parallel and perpendicular components of the wave vector $\mathbf{k}$, T_s is the temperature, $\rho_s = v_\perp/\Omega_s$ is the Larmor radius, $L_n = |\nabla \ln n_0|^{-1}$ is a characteristic scale length of the equilibrium density profile n_0. As shown in Fig. 2, the single particle motion under strong ambient fields consists of fast periodic gyro-motion and slow guiding-centre motion. Low frequency perturbations satisfying this ordering mainly affect the latter motion, and the magnetic moment, $\mu = m_s v_\perp^2/2B_0$, becomes an approximate adiabatic invariant. In analysing such a particle orbit, it is convenient to use the guiding-centre coordinates $\mathbf{Z}_{GC} = (t; \mathbf{R}, u, \mu, \alpha)$, where $\mathbf{R}$ is the guiding-centre position, α is the gyro-phase angle, $u = v_\parallel + (e_s/cm_s)A_\parallel$ is the generalised parallel velocity, $A_\parallel = \mathbf{b}\cdot\mathbf{A}_1$, and $v_\parallel = \mathbf{v}\cdot\mathbf{b}$ and $v_\perp = |\mathbf{v}\times\mathbf{b}|$ are parallel and perpendicular

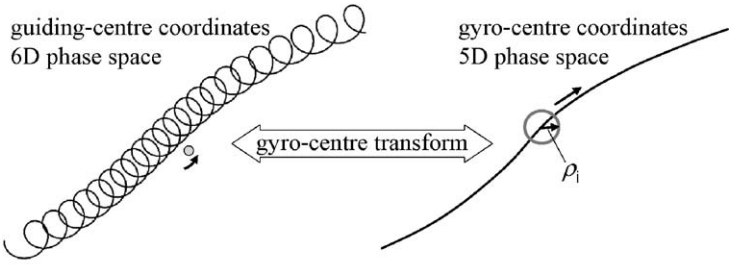

Fig. 2. By applying the gyro-centre transform, fast gyro-motion is eliminated, and the problem is reduced from 6D to 5D with keeping kinetic effects such as the finite Larmor radius effect.

components of the velocity, respectively. For a fusion plasma with finite but small β (typically $\beta \sim 1\%$), the perturbed field is given as $\mathbf{B}_1 = \nabla \times A_\parallel \mathbf{b}$, and the parallel component of $\mathbf{B}_1$ is often neglected compared to $\mathbf{B}_0$, where $\beta = (n_0 T_i + n_0 T_e)/(B_0^2/8\pi)$ is the ratio of the plasma kinetic pressure to the magnetic pressure. A transform of the Hamiltonian from $\mathbf{Z}_{\rm CC}$ to $\mathbf{Z}_{\rm GC}$ is systematically given by the guiding-centre transform [20], and we have

$$H_s = \frac{1}{2} m_s u^2 + \mu B_0 + e_s \Psi \tag{12}$$

where $\Psi = \phi - u A_\parallel / c$ is the generalised potential.

We then separate fast periodic gyro-motion and slow guiding-centre motion by applying the secular perturbation theory to the perturbed Hamiltonian (12), and find new coordinates, the gyro-centre coordinates $\mathbf{Z}_{\rm GY} = (t; \bar{\mathbf{R}}, \bar{u}, \bar{\mu}, \bar{\alpha})$, where an approximate invariant μ becomes an exact invariant $\bar{\mu}$ and its conjugate variable $\bar{\alpha}$ is seen as an ignorable coordinate. The gyro-centre transform valid up to $\mathcal{O}(\varepsilon_g)$ is given as

$$\mathbf{Z}_{\rm GY} = \mathbf{Z}_{\rm GC} + \{\tilde{S}, \mathbf{Z}_{\rm GC}\} + \mathcal{O}(\varepsilon_g^2) \tag{13}$$

where $\{\cdot, \cdot\}$ is the Poisson bracket in the gyro-centre coordinates [16],

$$\{F, G\} \equiv \frac{\Omega_s}{B}\left(\frac{\partial F}{\partial \alpha}\frac{\partial G}{\partial \mu} - \frac{\partial F}{\partial \mu}\frac{\partial G}{\partial \alpha}\right) + \frac{\mathbf{B}^*}{m_s B_\parallel^*} \cdot \left(\nabla F \frac{\partial G}{\partial u} - \frac{\partial F}{\partial u}\nabla G\right) - \frac{c}{e_s B_\parallel^*}\mathbf{b} \cdot \nabla F \times \nabla G \tag{14}$$

and $B_\parallel^* = \mathbf{b} \cdot \mathbf{B}^*$ is a parallel component of $\mathbf{B}^* = \mathbf{B}_0 + (B_0 \bar{u}/\Omega_s)\nabla \times \mathbf{b}$. The generating function $\tilde{S}$ is solved as

$$\tilde{S}(\mathbf{Z}_{\rm GC}, t) = \frac{e_s}{\Omega_s}\int^{\alpha} \left[\Psi - \langle \Psi \rangle_\alpha\right] \mathrm{d}\alpha' \tag{15}$$

where the gyro-average is defined as $\langle \cdot \rangle_\alpha \equiv \oint \cdot \, \mathrm{d}\alpha/2\pi$. This transform is formulated based on the Lie perturbation theory, so that the transform keeps an area preserving property of the Hamiltonian system up to arbitrary order in ε_g and the Poisson bracket becomes form invariant. Interested readers should refer to the literature for further details. After the transform, α-dependent non-secular perturbations are absorbed by the generating function $\tilde{S}$, and the Hamiltonian $\bar{H}_s$ becomes independent of $\bar{\alpha}$,

$$\bar{H}_s = \frac{1}{2} m_s \bar{u}^2 + \bar{\mu} B_0 + e_s \langle \Psi \rangle_{\bar{\alpha}} \tag{16}$$

We then have a reduced kinetic equation or a gyrokinetic equation, which describes an evolution of a guiding-centre distribution function $\bar{f}_s$ in 5D phase space,

$$\frac{D\bar{f}_s}{Dt} \equiv \frac{\partial \bar{f}_s}{\partial t} + \{\bar{f}_s, \bar{H}_s\} = \frac{\partial \bar{f}_s}{\partial t} + \{\bar{\mathbf{R}}, \bar{H}\} \cdot \frac{\partial \bar{f}_s}{\partial \bar{\mathbf{R}}} + \{\bar{u}, \bar{H}\}\frac{\partial \bar{f}_s}{\partial \bar{u}} = 0 \tag{17}$$

where the nonlinear characteristics, $\dot{\mathbf{Z}}_{\rm GY} = \{\mathbf{Z}_{\rm GY}, \bar{H}\}$, are given as

$$\frac{\mathrm{d}\bar{\mathbf{R}}}{\mathrm{d}t} = \bar{u}\mathbf{b} + \frac{c}{e_s B_\parallel^*}\mathbf{b} \times \left(e_s \nabla \langle \Psi \rangle_\alpha + m_s \bar{u}^2 \mathbf{b} \cdot \nabla \mathbf{b} + \bar{\mu} \nabla B_0\right) \tag{18}$$

$$\frac{\mathrm{d}\bar{u}}{\mathrm{d}t} = -\frac{\mathbf{B}^*}{m_s B_\parallel^*} \cdot \left(e_s \nabla \langle \Psi \rangle_{\bar{\alpha}} + \bar{\mu} \nabla B_0\right) \tag{19}$$

$$\frac{\mathrm{d}\bar{\mu}}{\mathrm{d}t} = 0 \tag{20}$$

The guiding-centre orbit (18) is determined by parallel thermal motion and perpendicular drift motion associated with the electromagnetic perturbation and the curvature and gradient of the magnetic field. In Eq. (19), the generalised parallel velocity suffers from acceleration forces associated with the electromagnetic perturbation and the gradient of the magnetic field. The latter force works as the magnetic mirror in the presence of two constants of motion in the unperturbed orbit, the energy $\varepsilon = m_s \bar{u}^2/2 + \bar{\mu} B_0$ and the magnetic moment $\bar{\mu}$. In Fig. 3, the unperturbed orbits show complicated trajectories depending on the pitch angle $\xi = \sin^{-1}(v_\perp/v)$ at the outboard mid-plane, and are classified mainly into passing and trapped particles. While passing particles are characterised by the parallel motion and the perpendicular magnetic drift, trapped particles show the bounce motion in the weak field side, and their magnetic

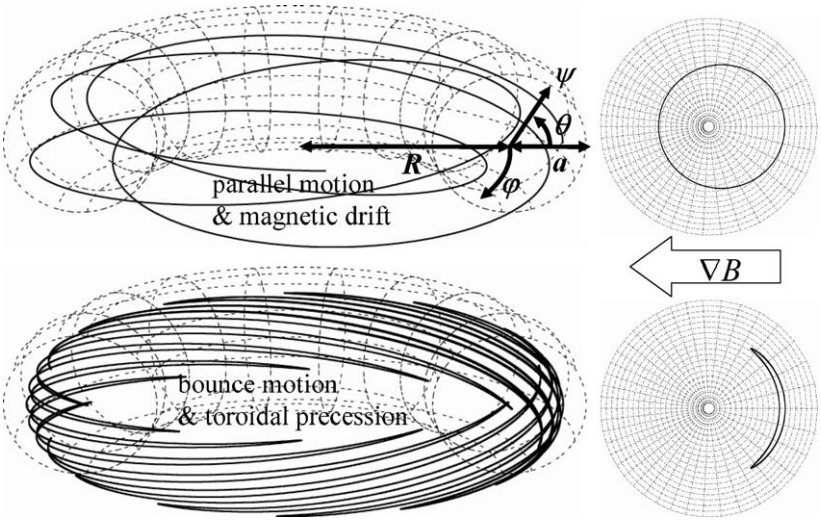

Fig. 3. Typical unperturbed guiding-centre orbits of passing and trapped particles, and their projection on the poloidal cross-section. The coordinates (ψ, θ, φ) show the radial direction, the poloidal angle, and the toroidal angle.

drift appears as the toroidal precession motion. On the poloidal plane, they show closed orbits, which corresponds to constant surfaces of the canonical toroidal angular momentum, $p_\varphi = -(e_s/c)\psi + m_s v_\parallel (\mathbf{B}_0 \cdot \nabla\varphi/|\nabla\varphi|^2)/B_0$, which is another constant of motion in the axisymmetric tokamak configuration. Therefore, the equilibrium solution of the gyrokinetic equation (17) is given as a function of three constants of motion, $f_{0s}(p_\varphi, \varepsilon, \bar{\mu})$. The parallel and perpendicular motion in the guiding-centre orbit is closely related to micro-instabilities, which are excited by density gradient, ion temperature gradient (ITG), and electron temperature gradient (ETG) through various wave-particle resonant interactions. Depending on the resonance condition, micro-instabilities are classified into slab modes, toroidal modes, and trapped particle modes, where the parallel motion of passing particles, the magnetic drift of passing particles, and the toroidal precession of trapped particles are essential for the wave-particle interaction, respectively. Detailed classification of micro-instabilities can be found in the literature [21–24]. On the other hand, these wave-particle interactions also works as a damping mechanism for smaller scale perturbations. Especially, high-$k_\parallel$ components suffer from the Landau damping due to the parallel motion of passing particles, which restricts turbulent structures to so-called flute-like structures with $k_\parallel \sim 0$.

Finally, the equation system is closed by imposing the self-consistency. f_s and $\bar{f}_s$ are related by the following pull-back transform valid up to $\mathcal{O}(\varepsilon_g)$,

$$f_s = \bar{f}_s + \{\tilde{S}, \bar{f}_s\} + \mathcal{O}\big(\varepsilon_g^2\big) \tag{21}$$

By substituting f_s to Eqs. (8) and (9), the gyrokinetic Poisson–Ampère law for the perturbed fields is obtained as

$$-\nabla^2\phi = \sum_s \left[4\pi e_s \int \bar{\delta} f_s \delta\big([\bar{\mathbf{R}} + \bar{\rho}_s] - \mathbf{x}\big) \mathcal{J}_s \, \mathrm{d}^6\bar{Z} - \frac{1}{\lambda_{Ds}^2}\big(\phi - \langle\bar{\phi}\rangle_\alpha\big) \right] \tag{22}$$

$$-\nabla_\perp^2 A_\parallel = \sum_s \left[\frac{4\pi e_s}{c} \int \bar{u}\bar{\delta} f_s \delta\big([\bar{\mathbf{R}} + \bar{\rho}_s] - \mathbf{x}\big) \mathcal{J}_s \, \mathrm{d}^6\bar{Z} - \frac{\omega_{ps}^2}{c^2}\langle\bar{A}_\parallel\rangle_\alpha \right] \tag{23}$$

where $\bar{\delta} f_s = \bar{f}_s - f_{0s}$, λ_{Ds} is the Debye length, ω_{ps} is the plasma oscillation frequency, $\mathcal{J}_s = m^2 B_\parallel^*$ is the Jacobian of the gyro-centre coordinates, and $\langle\bar{\cdot}\rangle_\alpha = \int \langle\cdot\rangle_\alpha f_{0s} \delta([\bar{\mathbf{R}} + \bar{\rho}_s] - \mathbf{x}) \mathcal{J}_s \, \mathrm{d}^6\bar{Z}/n_0$. The displacement current in Eq. (8) is neglected for low frequency phenomena considered here. The second term in the r.h.s. of Eqs. (22) and (23), which comes from $\{\tilde{S}, \bar{f}_s\}$, show gyrokinetic polarisation and magnetisation due to the finite Larmor radius effect. In deriving Eqs. (22) and (23), nonlinear polarisation and magnetisation effects, which are higher order in ε_g, are neglected. The gyrokinetic Vlasov–Maxwell system, Eqs. (17), (22), and (23), is a standard kinetic model to describe the micro-turbulence.

The most important feature of the gyrokinetic Vlasov–Maxwell system is that high frequency phenomena such as the Langmuir wave, ω_{ps}, and the Cyclotron wave, Ω_s, are eliminated with keeping essential kinetic effects for

low frequency micro-turbulence. From a point of view of the simulation, the limitations on the time step and the grid spacing are relaxed from $\Delta t\omega_{ps} < 1$ and $\Delta r < \lambda_{Ds}$ to $\Delta t\omega_s^* < 1$ and $\Delta r < \rho_s$, and the computational cost is significantly reduced. Another important feature is the conservation properties. Since the transform is designed to keep the Hamiltonian nature of the system, the gyrokinetic Vlasov–Maxwell system conserves the particle number, the momentum, the energy, and the entropy as in the Vlasov–Maxwell system. For Eqs. (17), (22), and (23), the total energy conservation is derived as

$$\frac{\mathrm{d}}{\mathrm{d}t}(E_k + E_\phi + E_{A_\parallel}) = 0 \tag{24}$$

$$E_k = \sum_s \left[\int \left(\frac{1}{2} m_s \bar{u}^2 + \bar{\mu} B_0 \right) \bar{f}_s \mathcal{J}_s \, \mathrm{d}^6 \bar{Z} \right] \tag{25}$$

$$E_\phi = \frac{1}{8\pi} \int |\nabla \phi|^2 \, \mathrm{d}^3 x + \frac{1}{8\pi} \sum_s \sum_{\mathbf{k}} \frac{1}{\lambda_{Ds}^2} \left[1 - \Gamma_0 \left(k_\perp^2 \rho_s^2 \right) \right] |\phi_{\mathbf{k}}|^2 \tag{26}$$

$$E_{A_\parallel} = \frac{1}{8\pi} \int |\nabla_\perp A_\parallel|^2 \, \mathrm{d}^3 x + \frac{1}{8\pi} \sum_s \sum_{\mathbf{k}} \frac{\omega_{ps}^2}{c^2} \Gamma_0 \left(k_\perp^2 \rho_s^2 \right) |A_{\parallel \mathbf{k}}|^2 \tag{27}$$

where $\phi = \sum_{\mathbf{k}} \phi_{\mathbf{k}} \exp(\mathrm{i}\mathbf{k} \cdot \mathbf{x})$, $A_\parallel = \sum_{\mathbf{k}} A_{\parallel \mathbf{k}} \exp(\mathrm{i}\mathbf{k} \cdot \mathbf{x})$, $\Gamma_0(b) = I_0(b)\mathrm{e}^{-b}$, and I_0 is the zeroth order modified Bessel function. An exact conservation property is important especially in studying nonlinear problems, where an analytic solution can hardly be found. The total particle and energy conservations are normally checked as a stringent test of the quality of the nonlinear simulation.

2.3. Kinetic fluid model

A fluid approach is the most commonly used approximation in describing turbulent fluids. A set of fluid equations is derived by taking the corresponding velocity moments of the Boltzmann equation. Since the electromagnetic perturbations are determined by the particle density and the current density, which are the zeroth and first order moments, a fluid model provides simple and useful means to analyse fluid phenomena, provided that a plasma is collisional and is close to a local thermodynamic equilibrium. The two component (ion and electron) fluid model, which is exactly valid for a collisional plasma, was derived in [25]. Under the quasi-neutrality condition, $n_i = n_e$, and the limit of $\omega/\Omega_s \sim \rho_s/L_n \sim (c/\omega_{ps})/L_n \to 0$, this model is reduced to a well-known single fluid MHD model, which is commonly used also in space plasma physics. However, in a high temperature collisionless fusion plasma, the collision frequency is much smaller than that of phenomena of interest (see Fig. 1), and a local thermodynamic equilibrium can not be assumed. In addition, the mean free path of particles $\sim$10 km is much larger than the plasma size $\sim$1 m, and the orbit effects due to the finite Larmor radius (see Fig. 2) and trapped particles (see Fig. 3) become important in analysing the micro-turbulence.

In general, the nth order moment equation involves the $(n+1)$th order moment term which comes from $\mathbf{v} \cdot \nabla f_s$ in the kinetic equation. A problem to close a set of fluid equations by approximating the $(n+1)$th order moment term using lower order moments is called as a closure problem. In the MHD model, the adiabatic law is often used, or the heat flux in the energy equation is modelled by the thermal conductivity term. However, such models may break down in the collisionless limit, because complicated velocity space structures in a particle distribution function are not fully characterised by lower order moments. Therefore, conventional fluid models are not enough to describe the micro-turbulence.

In order to resolve this problem, a kinetic fluid model such as the gyro-Landau fluid model has been developed. The gyro-Landau fluid model consists of moment equations of the gyrokinetic equation with dissipative [26] or non-dissipative [27,28] kinetic closure models which takes into account the linear wave-particle resonant interactions or the linear Landau damping. The model has been extended including the magnetic drift motion [29], the finite Larmor radius effect [30], bounce-averaged trapped particles [31], and the closure model with optimisation techniques to reproduce the linear wave dispersion of micro-instabilities [31]. The advantage of the kinetic fluid model is its lower computational cost than the gyrokinetic model. With the aid of this advantage, transport models were constructed based on database of kinetic fluid simulations over a broad parameter range [32,33]. However, a code benchmark project revealed that as for ion scale micro-turbulence driven by ITG (ITG turbulence), the gyro-Landau fluid model

gave 2–3 times higher transport levels than the gyrokinetic model [7]. This was partly explained by an insufficient modelling concerning to the trapped particle response to nonlinearly generated $E \times B$ zonal flows in the gyro-Landau fluid model [34], and efforts to fix this problem are ongoing [35]. Although the kinetic fluid model is useful to study qualitative physics, further improvements of the model are needed for quantitative estimation of the turbulent transport.

3. Numerical model

3.1. Particle and Vlasov approaches

The Lagrangian approach based on a Particle-In-Cell (PIC) method [36–38] has been a major approach in simulating collective phenomena in a collisionless plasma. In the PIC method, a plasma is expressed by relatively small number of super-particles with $e_{\rm SP} = \mathcal{M} e_s$, $m_{\rm SP} = \mathcal{M} m_s$, and $n_{\rm SP} = n_s/\mathcal{M}$, and their collective motion and the associated electromagnetic fields are treated in a straightforward manner using the Newton–Maxwell system for super-particles, which involves not only smoothly varying perturbations but also multiple particle interactions or collisions. In this sense, the system may be recognised as a collisional plasma described by the Boltzmann–Maxwell system, (1), (5)–(10). In the Boltzmann equation, the collective motion (the l.h.s. of Eq. (1)) is not changed by super-particles, while the collision term, which is characterised by the collision frequency $\nu_{ss} \sim \omega_{ps}/(n_0 \lambda_{Ds}^3)$, is artificially enhanced by $\mathcal{M}$ times. It is noted that the Vlasov equation or the collisionless limit is obtained in the opposite limit with $\mathcal{M} \to 0$. In order to reduce the enhanced numerical collision, the PIC method uses a finite size particle model, which works as a low-pass Fourier filter to weaken sub-grid scale thermal fluctuations or a particle noise. This model corresponds to the Debye shielding which screens short range forces in a collisionless plasma. Although the PIC method has been successfully applied to various kinetic phenomena in a collisionless plasma, it is essentially a model describing the Vlasov–Maxwell system and its application is limited for high frequency phenomena in a microscopic system. In a gyrokinetic particle model [39], the PIC method was extended for the gyrokinetic Vlasov–Maxwell system by replacing the Newton–Maxwell system with the nonlinear characteristics of the gyrokinetic equation and the gyrokinetic Poisson–Ampère law. In this model, limitations on the time step and the grid spacing are significantly relaxed, and low frequency phenomena can be simulated without a particle noise associated with gyro-motion. In spite of this low noise character, a remaining particle noise and its slow convergence property $\propto 1/\sqrt{n_{\rm SP}}$ were still problematic in simulating low amplitude micro-turbulence (typically $\delta n_s/n_0 \sim e_s\phi/T_s < 0.01$) in a macroscopic system such as a full torus configuration. To overcome this difficulty, the δf method [40,41] was proposed. In the δf method, a perturbed particle (or guiding-centre) distribution f_s is separated into an equilibrium distribution function f_{0s} and a nonlinear perturbation δf_s, and only δf_s is expressed by particles with the particle weight w_j, where w_j is defined as $w_j \equiv \mathcal{M} \int_{\mathcal{V}_j} \delta f_s \, {\rm d}^6 Z$ and $\mathcal{V}_j$ is the phase space volume around the jth particle. An evolution of δf_s is then solved along the nonlinear characteristics with self-consistent perturbed fields determined by Eqs. (22) and (23). The weighted particle is recognised as a Monte Carlo sampling of δf_s over phase space, and is often called as a marker particle or a tracer particle. In the δf method, the particle weight is reduced roughly by $\delta f_s/f_{0s} \sim \delta n_s/n_0 \sim 0.01$, and the simulation system becomes closer to the collisionless limit than the conventional PIC method. An evolution equation of δf_s is obtained by substituting $f_s = f_{0s} + \delta f_s$ to the kinetic equation,

$$\frac{D\delta f_s}{Dt} = -\{f_{0s}, H_s\} \tag{28}$$

Another simple way to evaluate δf_s is to use a constancy of f_s along the nonlinear characteristics,

$$\delta f_s\big(\mathbf{Z}(t)\big) = f_s\big(\mathbf{Z}(t_0)\big) - f_{0s}\big(\mathbf{Z}(t)\big) \tag{29}$$

where t_0 is the initial time. It was shown that both methods give almost the same results [42]. Since the δf method is a sort of Monte Carlo integration, its statistical property can be improved by optimising a distribution of sampling points or marker particles [41,43]. As seen in Eqs. (28) and (29), the δf method is constructed based on the property of the Liouville equation, which is satisfied in the conservative system without any source and collision terms. Thus, the δf PIC simulation is essentially a transient decaying turbulence simulation, where the conservative system is relaxed from a linearly unstable initial condition to a nonlinearly saturated state through nonlinear evolution of micro-instabilities. Extensions of the δf method including non-conservative effects such as the collision term [44,45] and the heat source [46,47] are in progress. Although toroidal particle simulations with the conventional PIC method were developed in

earlier works [48–50], the δf method has become a standard method in most of recent gyrokinetic toroidal particle simulations [8,51–56]. So far, most of δf PIC simulations have been restricted to an electrostatic simulation with adiabatic electrons. Electromagnetic problems require more delicate treatments because of a particle noise coming from fast electron motion. Improvements of the δf method towards an electromagnetic simulation are also in progress [56–60].

An alternative approach is the Eulerian (or Vlasov) approach, in which the kinetic equation is directly solved as a multi-dimensional partial differential equation using computational fluid dynamics schemes. One of the standard methods used in earlier works on the 1D Vlasov–Poisson system is the splitting method [61]. In this method, the Vlasov equation (5) is evolved at each time steps by tracing back the solution along the nonlinear characteristics as follows,

$$f_s^*(q,p) = f_s^n(q - p/m_s\Delta t/2, p) \tag{30}$$

$$f_s^{**}(q,p) = f_s^*(q, p - e_s\partial_q\phi^*\Delta t) \tag{31}$$

$$f_s^{n+1}(q,p) = f_s^{**}(q - p/m_s\Delta t/2, p) \tag{32}$$

where the upper subscript shows nth and intermediate time steps. The scheme is similar to the leap-frog scheme used in the PIC method and is sort of second order symplectic integration. Since the derivative terms are not explicitly evaluated as in a finite difference method, relatively large time step width, which is not limited by the numerical instability but by the numerical accuracy, is permitted. As an extension of this method for the gyrokinetic or drift-kinetic ($\rho_s \to 0$ limit) equation, the semi-Lagrangian method has been developed [62], and an application of this method to the micro-turbulence simulation is ongoing [63,64]. However, the rapid progress of computational power enabled the micro-turbulence simulation even with conventional finite difference and spectral approaches with explicit or semi-implicit time integration. Numerical schemes used in recent gyrokinetic toroidal Vlasov simulations are found in [65–68]. A Vlasov simulation has the following advantages. Firstly, it is free of a noise problem inherent to a particle simulation. Secondly, the numerical resolution in phase space is kept constant or controlled in a long time simulation, while a distribution of sampling points or marker particles in the δf PIC method changes in time following nonlinear characteristics. Thirdly, straightforward treatments of non-conservative effects such as source and collision terms are possible. Although the Eulerian approach has the above advantages which are essential for a long time simulation of experimentally relevant quasi-steady turbulent plasmas, this approach requires huge computational cost. Compared to a PIC simulation with $\sim$100 particles per a cell, a Vlasov simulation requires typically $\sim 10^4$ grids to resolve 2D velocity space. Because of this huge requirement on computational resources, a realistic micro-turbulence simulation via the Eulerian approach was difficult before developments of modern massively parallel supercomputers.

3.2. Global and flux tube approaches

A general description of the tokamak configuration consisting of nested magnetic surfaces labelled by the poloidal flux function ψ is written in a form [69],

$$\mathbf{B}_0 = \nabla\psi \times \nabla\big(q(\psi)\theta - \varphi\big) \tag{33}$$

where φ is the toroidal angle and θ is the straight-field line poloidal angle chosen so that the field line pitch, $q(\psi) = \mathbf{B}_0 \cdot \nabla\varphi / \mathbf{B}_0 \cdot \nabla\theta$, becomes constant on the magnetic surface. The flux coordinates are useful to represent flute like perturbations with $k_\parallel \simeq 0$ or $\mathbf{B}_0 \cdot \nabla h \simeq 0$. Since the tokamak configuration is periodic both in θ and φ, a perturbation $h(\psi,\theta,\varphi)$, can be expanded in a Fourier series,

$$h(\psi,\theta,\varphi) = \sum_{m,n} h_{mn}(\psi)\exp(\mathrm{i}m\theta - \mathrm{i}n\varphi) \tag{34}$$

where m and n are the poloidal and toroidal mode numbers. A flute like perturbation is then written as

$$\mathbf{B}_0 \cdot \nabla h = \mathbf{B}_0 \cdot \nabla\theta \sum_{m,n} \mathrm{i}\big(m - nq(\psi)\big)h_{mn}(\psi)\exp(\mathrm{i}m\theta - \mathrm{i}n\varphi) \simeq 0 \tag{35}$$

Since high $k_\parallel$ components far from the resonance condition, $m \simeq nq(\psi)$, suffer from strong Landau damping, a quasi 2D representation of flute like perturbations is possible,

$$h(\psi,\theta,\varphi) = \sum_n h_n(\psi,\theta)\exp\big(\mathrm{i}n\big[q(\psi)\theta - \varphi\big]\big) \tag{36}$$

where $h_n(\psi, \theta)$ is slowly varying in θ, reflecting variations of h in the direction of the magnetic field. Most of recent gyrokinetic simulations are efficiently implemented using this quasi 2D character. In addition, the magnetic moment $\bar{\mu}$ enters only parametrically in the gyrokinetic equation (17). Accordingly, in a discretised form, the gyrokinetic Vlasov–Maxwell system may be seen as a set of quasi 2D (ψ and φ) + 1D ($v_\parallel$) partial differential equations with different $\bar{\mu}$, which are coupled through the gyrokinetic Poisson–Ampère law.

The simplest and most realistic approach is a global model [8,48–52,54,55,67], in which the gyrokinetic Vlasov–Maxwell system is straightforwardly solved in a full torus geometry. In this model, global equilibrium profiles and their relaxation and evolution processes due to the turbulent transport and the particle, momentum, and heat sources are self-consistently treated. In the absence of these sources, the model is reduced to a conservative isolated system, where the particle number, the momentum, the energy, and the entropy are conserved. A global approach involves multi-scale physics ranging from the small scale turbulent fluctuations to the large scale profile variations. This multi-scale character is essential to study global profile effects which will be discussed later in association with the plasma size scaling of turbulent transport.

An alternative approach is a flux tube model [7,56,65,66,68], in which a local domain in the vicinity of a single field line is considered. This model assumes a multi-scale expansion with respect to a smallness parameter $\rho^* = \rho_s/a$ [39] or complete scale separation between turbulent fluctuations and equilibrium profiles, retaining the lowest order terms in ρ^*. Because of this local approximation, both an equilibrium quantity A and its radial derivative $\partial A/\partial\psi$ are assumed to be constant in the calculation domain. In addition, the model is described in the field aligned coordinates with a periodic radial boundary condition with phase shift reflecting the magnetic shear or the radial variation of the field line pitch $q(\psi)$ [70]. These assumptions are physically sound, provided that the radial correlation length of turbulent fluctuations is much shorter than the equilibrium scale length or the size of calculation domain. The flux tube model is a non-conservative open system developed to study local quasi-steady turbulent transport with fixed background profiles, and the system satisfies so-called entropy balance relation [71–73] instead of the conservation properties in the global model. The advantages of this approach is as follows. Firstly, the computational cost is significantly reduced compared to the global model. Because of this advantage, flux tube simulations are widely used in experimental data analyses. Secondly, the model is useful especially in studying electron turbulence and electromagnetic turbulence, which require treatments of multiple spatio-temporal scales coming from kinetic electron dynamics. Thirdly, because of aforementioned simplifications, the model is well established, and results from different codes are converged well. In contrast, the global model still has some ambiguities concerning to equilibrium profiles, source models, and boundary conditions, which make cross benchmarking among codes very difficult. The drawbacks of the flux tube model is obviously a lack of global profile effects. Especially, the plasma size dependence of the energy confinement time observed in the experiment can not be addressed using this model, because the model assumes an infinite plasma size from the beginning. In addition, recent global simulations disclosed formations of mesoscale structures in between the plasma size a and the Larmor radius ρ_s, which are sometimes beyond the limit of validity of the model.

Global simulations have been significantly advanced with increasing computational resources, and most of global codes have a capability of simulating the electrostatic ion turbulence with adiabatic electrons in a full torus configuration. However, a global simulation with electromagnetic perturbations and kinetic electrons is still prohibitive, and the flux tube approach is useful especially in understanding physics in such frontier issues, provided that its applicability is carefully checked. In addition to choice of a model, the validation of a simulation code is extremely important in view of complexity of physics involved in 5D gyrokinetic simulations. As stated earlier, the most fundamental validation is to check the first principles such as the conservation properties in the global model and the entropy balance relation in the flux tube model. In the next step, one can proceed to cross benchmarking among different codes. Finally, case comparisons with selected experiments would give feedback about missing physics in the simulation model.

4. Kinetic simulations of collisionless turbulent plasmas

4.1. Numerical dissipation in collisionless micro-turbulence simulation

A collisionless micro-turbulence simulation is recognised as DNS of the Hamiltonian (incompressible) flow in 5D phase space given by the gyrokinetic equation. In a sense, this may correspond to simulating ideal fluids described by the Euler equation. Although issues related to the entropy balance relation were successfully addressed

with non-dissipative Vlasov simulations based on an implicit symplectic scheme [74], in most of practical issues on the quasi-steady turbulent transport, numerical or physical dissipation is needed to avoid aliasing errors and numerical instabilities arising from filamentation or formation of fine scale structures in a long time simulation. In a particle simulation, similar course graining effects are naturally introduced by remaining numerical collisions among super-particles. Therefore, it is important to discuss effects of numerical dissipation on a collisionless micro-turbulence simulation. A plausible picture of a micro-turbulence simulation may be summarised as follows. Firstly, micro-instabilities are excited by inhomogeneities in a plasma through various wave-particle interactions as discussed earlier. Secondary, nonlinear mode coupling mainly due to the $E \times B$ nonlinearity transforms fluctuation field energy to linearly stable small scales typically given as $k_\perp \rho_i > 1$, where fluctuations are absorbed by the wave-particle interaction or the Landau damping. In general, an inertial spectral range as in neutral fluid turbulence is not expected in plasma turbulence, because both damping and forcing are determined by the wave-particle interaction and are distributed in a broad spectral range. Thirdly, the damped field energy is transferred to fine scales in the velocity space through the phase mixing, which comes from the ballistic motion or the parallel motion term in the kinetic equation. If one write the kinetic equation simply as $\partial_t f + v\partial_x f = 0$, an analytic solution of the ballistic mode, $f(x,v,t) = \sum_k f_{0k}(v)\exp(\mathrm{i}k[x - vt])$, is obtained for an initial condition, $f(x,v,t=0) = \sum_k f_{0k}(v)\exp(\mathrm{i}kx)$. Here, an effective wave number in the velocity space, kt, increases in time, and fine scale structures are continuously produced. Finally, such fine scale structures are eliminated by numerical or physical dissipation.

In [75,76], a role of the dissipation in determining quasi-steady turbulent transport was examined for the electrostatic ITG turbulence in a flux tube model without toroidal effects. In this limit, the gyrokinetic Vlasov–Poisson system yields

$$\partial_t \delta f_i + v_\parallel \nabla_\parallel \delta f_i + \mathbf{v}_{E\times B}\cdot\nabla\delta f_i = \left[-\mathbf{v}_{E\times B}\cdot\nabla \ln n_0\left\{1+\eta_i\left(\frac{m_i v_\parallel^2/2+\mu B}{T_i}-\frac{3}{2}\right)\right\} - \frac{e}{T_i}v_\parallel\nabla_\parallel\langle\phi\rangle_\alpha\right] f_M + C(\delta f_i) \tag{37}$$

$$\frac{1}{\lambda_{Di}^2}\left[\phi - \langle\bar{\phi}\rangle_\alpha\right] + \frac{1}{\lambda_{De}^2}\left[\phi - \langle\phi\rangle_{k_\parallel=0}\right] = 4\pi e\int \delta f_i \delta\big([\mathbf{R}+\rho_i]-\mathbf{x}\big)\mathcal{J}_i\,\mathrm{d}^6Z \tag{38}$$

where a notation of the gyro-centre coordinates $\bar{\cdot}$ is ignored for simplicity, the equilibrium distribution function is given by the Maxwellian distribution, $f_M = n_0(2\pi m_i T_i)^{-3/2}\exp[-(m_i v_\parallel^2/2+\mu B_0)/T_i]$, $\mathbf{v}_{E\times B} = (c/B_0)\mathbf{b}\times\nabla\langle\phi\rangle_\alpha$ is the $E\times B$ drift velocity, $\eta_i = |\nabla\ln T_i|/|\nabla\ln n_0|$, and $C(\delta f_i)$ is a collision term. In Eq. (37), the higher order parallel nonlinearity, $\nabla_\parallel\langle\phi\rangle_\alpha\partial_{v_\parallel}\delta f_i$, is neglected compared to the $E\times B$ nonlinearity, $\mathbf{v}_{E\times B}\cdot\nabla\delta f_i$. In Eq. (38), the quasi-neutrality condition is imposed by neglecting the l.h.s. of Eq. (22) compared to the ion polarisation term. An electron response is assumed to be adiabatic or the Boltzmann distribution, $n_e = n_0 + n_0 e\phi/T_e$, because the phase velocity of ion drift waves is much slower than the electron thermal velocity, $\omega_i^*/k_\parallel \sim v_{ti} \ll v_{te}$. It is noted that the adiabatic electron response, which comes from the parallel dynamics, vanishes for $k_\parallel = 0$ or magnetic surface averaged components, $\langle\phi\rangle_{k_\parallel=0}$. The entropy balance relation among the entropy variable δS, the fluctuation field energy W, the ion heat flux Q_i, and the collisional dissipation D is then derived by multiplying $\delta f_i/f_M$ to Eq. (37) and integrating it over phase space,

$$\frac{\mathrm{d}}{\mathrm{d}t}(\delta S + W) = Q_i + D_i \tag{39}$$

$$\delta S = \frac{1}{2}\int \frac{\delta f_i^2}{f_M}\mathcal{J}_i\,\mathrm{d}^6Z \tag{40}$$

$$W = \frac{1}{2}\sum_{\mathbf{k}}\left[1-\Gamma_0\big(k_\perp^2\rho_{ti}^2\big)\right]\left|\frac{e\phi_{\mathbf{k}}}{T_i}\right|^2 n_0 + \frac{1}{2}\frac{T_i}{T_e}\sum_{k_\parallel\neq 0}\left|\frac{e\phi_{\mathbf{k}}}{T_i}\right|^2 n_0 \tag{41}$$

$$Q_i = -\frac{1}{2T_i}\left[\int \mathbf{v}_{E\times B} n_0 \delta T_i\,\mathrm{d}\mathbf{R}\right]\cdot\nabla\ln T_i \tag{42}$$

$$D_i = \int C(\delta f_i)\frac{\delta f_i}{f_M}\mathcal{J}_i\,\mathrm{d}^6Z \tag{43}$$

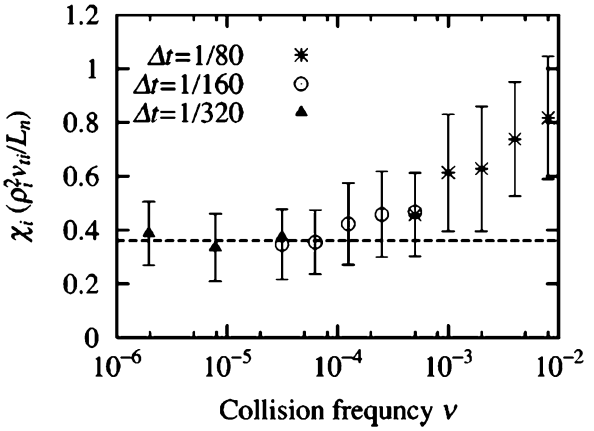

Fig. 4. The turbulent heat transport coefficients $\chi_i/(\rho_{ti}^2 v_{ti}/L_n)$ observed in slab ITG turbulence simulations ($E \times B$ zonal flows are turned off) with different collision frequencies $\nu/(v_{ti}/L_n)$ [76].

where $\delta T_i = \int m v_\parallel^2 \delta f_i \mathcal{J}_i \, \mathrm{d}v_\parallel \, \mathrm{d}\mu / n_0$. In the collisionless limit with $D_i \to 0$, Eq. (39) suggests two scenarios. One is a statistically steady state with no heat flux, $Q_i = 0$, and $\dot{\delta S} = \dot{W} = 0$. The other is a quasi-steady turbulent state with $\dot{\delta S} = Q_i = \text{const}$ and $\dot{W} = 0$. In the latter scenario, continuous growth of fine scale structures in the velocity space or higher order velocity moments contributes to monotonic increase of δS, while W and Q_i characterised by the lower order velocity moments stay in steady values. In [75], both scenarios were identified in ITG turbulence simulations with and without $E \times B$ zonal flows, which are nonlinearly generated from turbulent fluctuations. Although the former scenario is trivially satisfied in a linearly stable plasma, the simulation showed that it can be realized even in a linearly unstable plasma. In the simulation with $E \times B$ zonal flows, the heat flux Q_i is quenched in a nonlinearly saturated steady state, provided that $E \times B$ zonal flows grow strong enough to suppress the ITG turbulence. On the other hand, the simulation without $E \times B$ zonal flows showed the latter scenario with a quasi-steady heat flux, in which δS grows monotonically until fine scale structures reach at the limit of velocity space resolution. This suggests that a long time micro-turbulence simulation is prohibited without numerical or physical dissipation.

In [76], a relation between the dissipation D_i and the turbulent transport Q_i was studied by adding the collisional dissipation to the latter scenario. In this case, δS also keeps a quasi-steady value because of elimination of fine scale structures via the collisional dissipation, and the turbulent transport is balanced with the collisional dissipation, $Q_i + D_i = 0$. This relation looks as the turbulent transport is determined by the collision frequency. However, it was also found that in a weak collisional regime, the turbulent transport approaches to the collisionless limit asymptotically (see Fig. 4). To understand this result, properties of the turbulent spectrum in the $v_\parallel$ space was investigated in detail, and the following properties were clarified. Firstly, the turbulent spectrum has a subrange of the $v_\parallel$ spectrum which is free from the entropy production and the collisional dissipation. Secondly, the turbulent cascade in the subrange is similar to that of the passive scaler convection beyond the Kolmogorov scale in turbulent fluids with a large Prandtl number [77]. Thirdly, if dissipation scales in the $v_\parallel$ space is small enough, the dissipation process does not affect lower order velocity moments, which dictate W and Q_i. These findings support the hypothesis that forcing determines dissipation [72]. Therefore, a collisionless micro-turbulence simulation is possible with finite resolution available on the present-day supercomputers, provided that numerical dissipation in a Vlasov simulation or numerical collisions in a particle simulation are finite but small enough. A careful convergence study against grid size or a number of marker particles is essential to validate this point.

4.2. Zonal flows in ITG turbulence

The ITG turbulence is believed to be a plausible mechanism of ion heat transport in fusion plasmas and has been intensively studied using gyrokinetic and gyro-fluid simulations since early 90s. One of the most significant outcomes from those ITG turbulence simulations is a discovery of $E \times B$ zonal flows, which was discussed in a recent review [9]. In an axisymmetric tokamak configuration, $E \times B$ zonal flows are defined as azimuthally symmetric ($m = n = 0$) and radially varying potential perturbations produced nonlinearly from turbulent fluctuations. Since their $E \times B$ drift

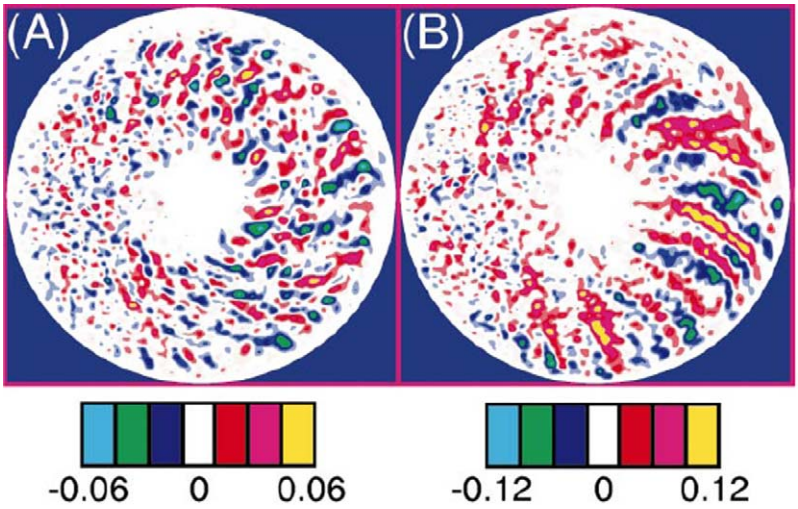

Fig. 5. Contour plots of $e\phi/T_i$ on the poloidal (r–θ) plane. (A) and (B) show the turbulent structures observed in the steady state of ITG turbulence simulations with and without $E \times B$ zonal flows [54]. In (A), dominant zonal flow components are filtered out to highlight the differences in the turbulent eddy size.

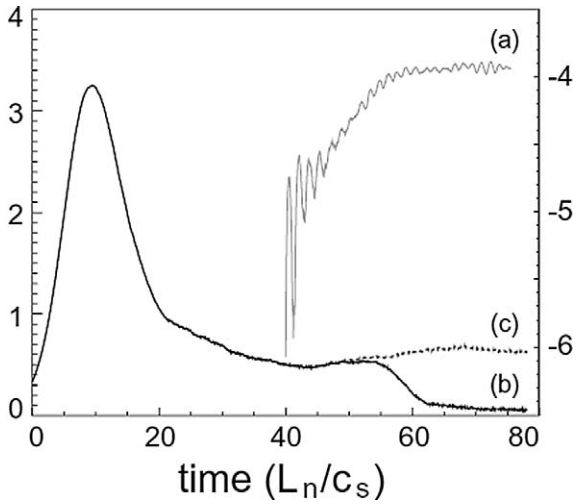

Fig. 6. The ion heat diffusivity χ_i (linear scale) observed in ITG turbulence simulations with (b) and without (c) $E \times B$ zonal flows [96]. In (b), $E \times B$ zonal flows are turned on at $tc_s/L_n \sim 40$. (a) shows a time evolution of the zonal flow amplitude $v_{E\times B}$ (log scale).

velocity is directed within the magnetic surface, which is also constant T_i, T_e, and n_0 surfaces to the lowest order in ρ^*, they do not contribute to particle and heat transport. Moreover, they suppress the turbulence and associated transport by shearing processes of turbulent eddies, which reduce the radial correlation length and enhance coupling to linearly stable small scale fluctuations. Fig. 5 shows ITG turbulence simulations with and without $E \times B$ zonal flows. In the tokamak configuration, the ITG turbulence tends to form radially elongated vortex structures, which balloon in the weak field side (see Fig. 5(B)). However, in Fig. 5(A), such ballooning structures are broken up by $E \times B$ zonal flows, leading to shorter radial correlation length and lower saturation levels. In Fig. 6, the turbulent transport is dramatically reduced by $E \times B$ zonal flows. In general, turbulence suppression by mean and zonal $E \times B$ shear flows is an essential ingredient in various improved confinement phenomena in a fusion plasma [78–82]. The criterion for turbulence suppression was formulated as $\gamma_E \sim \tau_c^{-1}$, where τ_c is the correlation time of turbulent fluctuations, and the shearing rate, γ_E, is defined by the decorrelation time of neighbouring fluid elements separated by the turbulent correlation length, l_c [83,84]. This criterion is often replaced by an empirical rule, $\gamma_E \sim \gamma_L$, found in gyrofluid simulations with equilibrium $E \times B$ shear flows [85], where γ_L is the linear growth rate in the absence of $E \times B$ shear flows. It was also

reported that the shearing rate of $E \times B$ zonal flows observed in the ITG turbulence is comparable to this empirical rule [86–88].

Zonal flows are universal phenomena not only in the drift wave turbulence in a fusion plasma but also in the Rossby wave turbulence or the β-plane turbulence in the planetary atmosphere. Since the reduced model of the drift wave turbulence, the Hasegawa–Mima equation [92], is mathematically identical to that of the Rossby wave turbulence, the Charney equation [93], their similarities have been often discussed in the literature [9,79,89–91]. In the 2D limit with $k_\parallel \to 0$, the gyrokinetic Vlasov–Poisson system, (17) and (22), yields the Hasegawa–Mima equation,

$$\partial_t\left(\nabla^2\phi - \phi\right) - \nabla\phi \times \mathbf{b} \cdot \nabla\left(\nabla^2\phi - \ln n_0\right) = 0 \tag{44}$$

where normalisations are chosen as $t\Omega_i \to t$, $\rho_s\nabla \to \nabla$, and $e\phi/T_e \to \phi$ with $\rho_s = \sqrt{T_e/T_i}\rho_{ti}$. Here, the homogeneous magnetic field, adiabatic electrons, $k_\perp^2\rho_{ti}^2 \ll 1$, and $\lambda_{Di}^2/\rho_{ti}^2 \ll 1$ are also assumed. Eq. (44) is the simplest model describing 2D turbulence in rotating fluids. In a fusion plasma, quasi-2D character comes from anisotropic turbulent structures with $k_\parallel/k_\perp \sim \mathcal{O}(\varepsilon_g)$ produced by strong confinement fields. The diamagnetic rotation, $\mathbf{v}^* = \mathbf{b} \times \nabla \ln n_0$, corresponds to the β effect or the north–south gradient of Coriolis frequency in the planetary atmosphere. It is noted that in this subsection, we use β differently from other sections to discuss the 2D rotating fluid turbulence following notations in the literature. Despite such similarities in the model equation, a generation mechanism of $E \times B$ zonal flows in the ITG turbulence seems to be different from that of east–west zonal jets in the planetary atmosphere. In the Rossby wave turbulence, zonal flow generation is often explained by the self-organisation via the turbulent spectral cascade. In the 2D fluid turbulence which conserves the energy and the potential enstrophy, resonant three wave coupling due to the nonlinearity produces the inverse energy cascade [94]. However, in the 2D rotating fluid turbulence, the wave dispersion, $\omega = \beta k_y/(1 + k_\perp^2)$, produced by the β effect leads to resonant detuning, which suppresses the inverse energy cascade in large scales, and anisotropic spectra with zonal flows are formed at the boundary separating turbulence and wave dominated regimes [95], where $\beta = |\nabla \ln n_0|$ and $k_y = \mathbf{b} \times (-\nabla n_0/|\nabla n_0|) \cdot \mathbf{k}$. In contrast, zonal flow generation in the ITG turbulence is characterised by shear flow instabilities. In Fig. 6, $E \times B$ zonal flows are evolved from a quasi-steady state of the ITG turbulence as shown in Fig. 5(B), and an exponential growth of $E \times B$ zonal flows are clearly seen. This zonal flow instability was discussed based on a parametric instability among zonal flows and coherent pump waves [97], a modulational instability driven by the Reynolds stress of the drift wave spectrum [98], and a Kelvin–Helmholtz (KH) type instability of radial $E \times B$ shear flows involved in radially elongated vortices [99].

The ITG turbulence is different from the Rossby wave turbulence in the following points. Firstly, in contrast to the potential vorticity of turbulent components, $(1 + k_\perp^2)\phi_{\mathbf{k}}$, that of $m = n = 0$ component is given as $k_\perp^2\phi_{\mathbf{k}}$, because of the absence of an adiabatic electron response to $k_\parallel = 0$ component. This special response of adiabatic electrons makes effective inertia of $k_\parallel = 0$ zonal flow components much smaller than that of $k_\parallel \neq 0$ turbulent components. This feature makes coupling to $m = n = 0$ component remarkably strong, and enhances zonal flow instabilities in the ITG turbulence [100,101]. Secondly, in a typical magnetic configuration with the magnetic shear, turbulent structures have 3D character consisting of multiple helicity perturbations excited at each resonant surfaces with $q(\psi) = m/n$. In Fig. 6, $E \times B$ zonal flows are excited even with the magnetic shear. The magnetic shear is important also from a point of view of the KH instability, which is one of relevant mechanisms of zonal flow saturation [99,102–104]. In inviscid fluids, the KH instability is universally unstable for zonal flows which have inflection points of the flow shear, provided that the system size is large enough to cover the unstable spectrum. The β effect potentially has a stabilising effect by an effective zero point shift of the flow curvature [79]. In addition, the magnetic shear produces another stabilising effect induced by the parallel dynamics, which plays a similar role as a stabilising effect of buoyancy on the KH instability in a neutral fluid [102]. Thirdly, the wave dispersion of the ITG turbulence is relatively weak, because its linearly unstable range, $k_\perp < 1$, is much lower than typical forcing ranges of the Rossby wave turbulence, $k_\perp \gg 1$. Because of the weak dispersion and the 3D turbulent character, the self-organisation as in the Rossby wave turbulence may not be expected in the ITG turbulence. Finally, inhomogeneous toroidal magnetic fields (typically given as $B_\varphi \sim B_0[1 + r/R\cos(\theta)]$) provide linear mode coupling among $m = n = 0$ and $m \neq 0$, $n = 0$ components through the magnetic drift motion. While KH stable $E \times B$ zonal flows are a possible equilibrium solution in slab or cylindrical plasmas, they are damped in a toroidal plasma through linearly coupled $k_\parallel \neq 0$ modes, which suffer from the Landau damping. However, ITG turbulence simulations with different L_{ti} found that near marginal stability, there exists a parameter regime where the ITG turbulence is linearly unstable but is nonlinearly quenched by self-generated $E \times B$ zonal flows [7]. From a point of view of the entropy balance relation, such a nonlinear state is seen

as a collisionless steady solution with no turbulent transport. This nonlinear up shift of effective marginal stability shed light on the importance of understanding a mechanism to sustain $E \times B$ zonal flows in a toroidal plasma without turbulence drive. A linear kinetic analysis in [34] showed that initially given $E \times B$ zonal flows are not completely damped in a collisionless plasma, and residual flows which are not subject to the Landau damping are determined by a polarisation effect of trapped particles. The residual flow level predicted by this theory was recovered in many gyrokinetic simulations [7,55,67,68,105,106] and is becoming a standard linear benchmark test to check kinetic responses of the simulation against $E \times B$ zonal flows. As an ultimate damping mechanism of the residual $E \times B$ zonal flows, an importance of collisional zonal flow damping was emphasised in [9,107,108]. A determination of $E \times B$ zonal flows is such a delicate problem consisting of nonlinear turbulence drive, the KH instability, collisionless and collisional zonal flow damping, and trapped particle dynamics. It was also pointed out that use of the conservative gyrokinetic Vlasov–Maxwell system with particle number conservation [109] and an exact equilibrium distribution function reflecting toroidal symmetry [55] is essential in simulating such complicated zonal flow physics.

4.3. Advances in gyrokinetic simulation

From a point of view of fusion engineering, the final goal of the micro-turbulence simulation is quantitative estimation and prediction of turbulent transport in fusion plasmas. Developments of modern massively parallel supercomputers and advanced simulation models significantly enhanced capabilities of gyrokinetic simulations towards more realistic plasma parameters, geometry, and physical effects. Especially, increasing computational resources benefited parametric studies associated with the size scaling of turbulent transport, which is one of critical issues in predicting confinement performances in future large devices. The conventional turbulent transport theories assume a simple local turbulence picture, in which the turbulent correlation length scale with the Larmor radius, $l_c \sim \rho_i$, and the correlation time is replaced by the linear growth time, $\tau_c \sim \gamma_L^{-1} \sim a/c_s$, leading to so-called gyro-Bohm like scaling, $\chi_{\mathrm{GB}} \sim l_c^2/\tau_c \sim c_s \rho_i^2/a$, where $c_s = \sqrt{T_e/m_i}$ is the sound velocity. Although recent experimental observations support the above assumptions on l_c and τ_c [110], the ion heat diffusivity observed in low confinement plasmas called as L-mode plasma showed much worse size scaling, $\chi_B \sim c_s \rho_i \sim \chi_{\mathrm{GB}}/\rho^*$, which is often called as Bohm like [110–112]. This indicated that the experiment cannot be fully described by a local turbulence picture, and that a global approach is essential to study the size scaling. In fact, many global gyrokinetic simulations of the ITG turbulence have shown Bohm like size scaling so far [47,49,50,52,88,113,114], and its mechanism has been explained mainly based on profile shear effects and turbulence spreading. The former effect has two aspects. One is the shear of mode phase velocity typically given by the diamagnetic rotation velocity, $v^* = (cT_i/eB_0)|\nabla \ln n_0|$, which suppress coupling between perturbations excited at separate resonant surfaces and limits the envelope width of linear ballooning structures as $\Delta r \sim \sqrt{\rho_i a}$ [115–117]. Although this envelope width naturally gives Bohm like scaling, linear ballooning structures are easily broken up by $E \times B$ zonal flows as shown in Fig. 5(a). Another profile shear effect is stabilisation due to equilibrium $E \times B$ shear flows, which are dictated by a force balance relation derived from the ion momentum equation,

$$E_r = \frac{1}{en_0} \nabla P_i + U_\varphi B_\theta - U_\theta B_\varphi \tag{45}$$

where E_r is the equilibrium radial electric field, P_i is the ion pressure, U_φ (U_θ) and B_φ (B_θ) are the equilibrium flow velocity and the magnetic field in the toroidal (poloidal) direction, respectively. In the case without equilibrium flows, the $E \times B$ shear flow is balanced with the diamagnetic rotation, and its shearing rate γ_E scales with ρ^*. It was shown that when the system is close to the turbulence suppression criterion, $\gamma_E \sim \gamma_L$, ρ^*-dependence of γ_E provides Bohm like scaling [88,118]. However, Bohm like scaling was observed even in the cases where the system is far above the criterion, $\gamma_E \ll \gamma_L$ [47], or E_r is dominated by other ρ^*-independent effects such as U_φ given by outer momentum input [114]. Such results were explained mainly by spreading of turbulent fluctuations into stable or less unstable regions, leading to lower intensity of fluctuation amplitudes. The turbulence spreading becomes less important as the plasma size increases, because its elementally processes are characterised by microscale or mesoscale phenomena such as avalanches between excitations of micro-instabilities and formations of steep gradient regions [119], avalanches due to KH like instabilities followed by formations of $E \times B$ zonal flows [102], and nonlocal

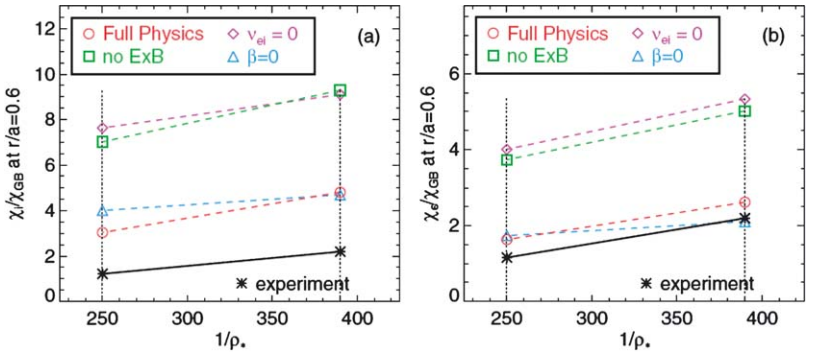

Fig. 7. Selected physical effects on (a) ion and (b) electron heat transport, and comparison with experimental estimates from [114].

modulational process between drift waves and zonal flows [120]. In general, all these profile shear effects vanishes in the large plasma size limit or $\rho^* \to 0$. In this sense, a local turbulence picture such as the flux tube model may give the upper limit of the turbulent transport. In fact, recent large scale global gyrokinetic simulations showed a favourable trend, that is, transition of the size scaling from Bohm like to gyro Bohm like in sufficiently large plasma size parameters [47,121].

In addition to the capability of simulating large size plasmas, the simulation model itself has been greatly improved including following physical effects. Firstly, shaped magnetic field configuration, which is adopted in most of recent advanced tokamak experiments, potentially has stabilising effects by changing the magnetic drift motion [122]. Secondly, kinetic electron responses are important to simulate electron turbulence driven by trapped electrons, the trapped electron mode (TEM) turbulence [21–24]. The TEM turbulence is coupled with the ITG turbulence in the same k range, and they are often called as the ITG-TEM turbulence. Since ion scale turbulence satisfy the quasi-neutrality condition, an inclusion of electron turbulence is essential to study particle transport. In addition, a reduction of an adiabatic electron response possibly affects zonal flow dynamics. Thirdly, electromagnetic perturbations provide a stabilising effect on the ITG mode and excite kinetic Alfvèn waves with increasing β [123]. Finally, electron–ion collisions affect the ITG-TEM turbulence by effective reduction of trapped electron drive [124]. In [114], gyrokinetic simulations including all these effects were compared against the ρ^* scan experiments in DIII-D tokamak [110], and it was shown that the ion and electron heat diffusivity and its ρ^*-dependence became closer to the experiment with adding more physical effects, notably equilibrium $E \times B$ shear flows and electron–ion collisions (see Fig. 7). Further investigations on physics related to particle transport, zonal flow dynamics, β scaling of turbulent transport in the ITG-TEM turbulence are ongoing [125–129].

Although suppression of ion scale micro-turbulence by $E \times B$ shear flows is one of most plausible mechanisms for ion heat transport barriers, the electron heat transport may not be explained only by ion scale micro-turbulence, because the electron heat diffusivity is universally anomalous even when the suppression condition, $\gamma_E \sim \gamma_L$, is satisfied for ion scale micro-instabilities such as the TEM. This fact suggests relevance of a short wavelength electron scale micro-instability driven by ETG (the ETG turbulence) which is isomorphic to the ITG turbulence and has higher characteristic frequency, growth rate, and wavenumber by $\sqrt{m_i/m_e}$. In such short wavelength regime, ions respond to fluctuations adiabatically due to the finite Larmor radius effect. It is noted that in contrast to the adiabatic electron response coming from parallel dynamics, the ion adiabatic response due to the perpendicular gyro-motion shields both $k_\parallel = 0$ and $k_\parallel \neq 0$ components with $k_\perp^2 \rho_i^2 \gg 1$, leading to relatively weak zonal flow excitation. Because of this feature, the ETG turbulence shows structure formations different from the ITG turbulence, and its turbulent structures are dramatically changed depending on the magnetic field configuration, namely the magnetic shear (see Fig. 8). Recent gyrokinetic simulations of the ETG turbulence found streamers or radially elongated vortices in the moderate magnetic shear [66,130–132] and zonal flows or poloidally elongated vortices in the weak magnetic shear [130]. Especially in the moderate magnetic shear, larger radial correlation lengths of streamers lead to enhanced electron heat transport than estimations from conventional transport theories assuming $l_c \sim \rho_e$. Although this feature is qualitatively consistent with the experiment, investigations on quantitative transport levels and physical mechanisms to determine turbulent structures are still in progress.

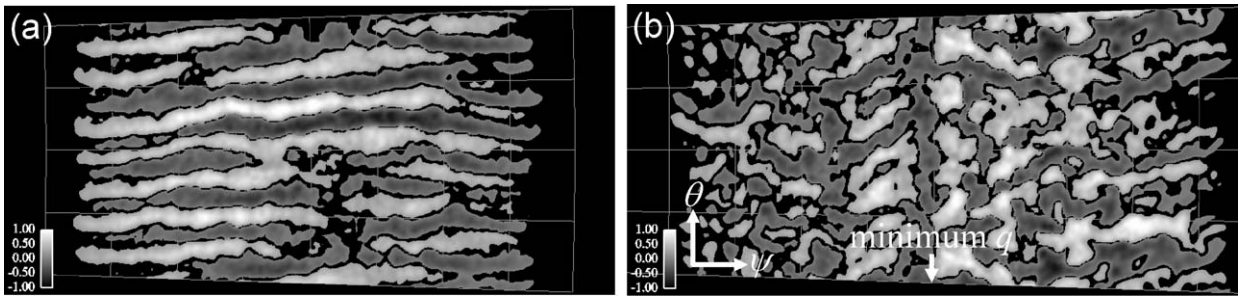

Fig. 8. Contour plots of ϕ observed at the outboard mid-plane, $\theta \sim 0$, in ETG turbulence simulations with (a) positive magnetic shear and (b) reversed magnetic shear where the sign of q' is changed across the minimum q surface. While the electron heat transport is enhanced by streamers in (a), it is significantly suppressed by zonal flows near the minimum q surface in (b) [130].

5. Discussion and future issues

With increasing computational resources and improved simulation models, kinetic simulations of collisionless turbulent plasmas have been established as an essential tool for studying tokamak turbulent transport. Recent gyrokinetic simulations disclosed rich physics behind tokamak turbulent transport and succeeded in reproducing heat transport observed in selected experiments. However, the present physics understanding is mainly on the steady ion heat transport caused by electrostatic fluctuations in conventional tokamak configurations, and further investigations are needed to answer the following outstanding issues. Firstly, understanding of the electron heat transport, the particle transport, and the momentum transport has not matured compared to that of the ion heat transport. In a burning plasma where the primary heating goes to electrons, the electron heat transport becomes particularly important. Although this issue has been discussed independently based on the ion (ρ_i) scale ITG-TEM turbulence and the electron (ρ_e) scale ETG turbulence under implicit assumption of scale separation, simultaneous treatment of ion and electron scale turbulence may be needed to determine the turbulent spectrum which causes the electron heat transport. Understanding of the particle transport is essential not only in predicting an electron density profile but also in estimating transport of impurities and helium ash leading to fuel dilution. The momentum transport is closely related to toroidal plasma rotation, which plays a critical role in stabilising MHD instabilities. Understanding of the momentum transport is highly desirable in predicting toroidal rotation especially in future large devices where enough outer momentum input is not assured. Secondly, study of the electromagnetic turbulence is needed to understand transport properties in a high β regime, where turbulent transport is dominated by kinetic Alfvèn waves rather than drift waves. Although electromagnetic perturbations were implemented in several gyrokinetic simulations, most of simulations were limited for a low β regime where turbulent fluctuations essentially have electrostatic character. An electromagnetic gyrokinetic simulation in a high β regime is of interest also from a point of view of an extension of the MHD theory including kinetic effects. Thirdly, improved confinement phenomena or transport barriers observed in recent advanced tokamak configurations are yet to be fully understood. If one assume equilibrium profiles with steep pressure gradients and associated $E \times B$ shear flows in transport barriers, improved confinement can be qualitatively explained based on turbulence suppression by $E \times B$ shear flows. However, a mechanism of such profile formations or transition to an improved confinement regime is still an open question. Although most of present gyrokinetic simulations are a decaying turbulence simulation or a driven turbulence simulation with fixed equilibrium profiles, a long time simulation involving evolutions of equilibrium profiles with particle, momentum, and heat sources may be needed to address interactions between transient turbulent transport and profile formations. All these issues are challenges for gyrokinetic simulations in extending capabilities to include multiple spatio-temporal scales and multiple physics. Towards reactor relevant micro-turbulence simulations, further advances in computer technology and simulation models are desirable.

Acknowledgements

We would like to thank Dr. X. Garbet for his support. One of the authors (Y.I.) acknowledges to Drs. S. Tokuda, M. Kikuchi, and M. Azumi for useful suggestions. The authors are supported by the Japanese Ministry of Education, Culture, Sports, Science, and Technology (Nos. 15760630, 16560727, and 17360445) and in part by the NIFS Collaborative Research (NIFS04KDAD003).

References

[1] F.L. Hinton, R.D. Hazeltine, Rev. Mod. Phys. 48 (1976) 239.
[2] S.P. Hirshman, D.J. Sigmar, Nucl. Fusion 21 (1981) 1079.
[3] ITER Physics Expert Groups on Confinement and Transport and Confinement Modelling and Database, Nucl. Fusion 39 (1999) 2175.
[4] A. Yoshizawa, et al., Plasma Phys. Control. Fusion 43 (2001) R1.
[5] J.A. Krommes, Phys. Rep. 360 (2002) 1.
[6] W.M. Tang, V.S. Chan, Plasma Phys. Control. Fusion 47 (2005) R1.
[7] A.M. Dimits, et al., Phys. Plasmas 7 (2000) 969.
[8] L. Villard, et al., Plasma Phys. Control. Fusion 46 (2004) B51.
[9] P.H. Diamond, et al., Plasma Phys. Control. Fusion 47 (2005) R35.
[10] S. Ichimaru, Statistical Plasma Physics, vol. I: Basic Principles, Addison–Wesley, Redwood City, CA, 1992.
[11] E.A. Frieman, L. Chen, Phys. Fluids 25 (1982) 502.
[12] D.H.E. Dubin, et al., Phys. Fluids 26 (1983) 3524.
[13] T.S. Hahm, W.W. Lee, A. Brizard, Phys. Fluids 31 (1988) 1940.
[14] T.S. Hahm, Phys. Fluids 31 (1988) 2670.
[15] A.J. Brizard, J. Plasma Phys. 41 (1989) 541.
[16] A.J. Brizard, Phys. Plasmas 2 (1995) 459.
[17] H. Sugama, Phys. Plasmas 7 (2000) 466.
[18] S. Wang, Phys. Rev. E 64 (2001) 056404.
[19] J.R. Cary, Phys. Rep. 79 (1981) 129;
J.R. Cary, R.G. Littlejohn, Ann. Phys. 151 (1983) 1.
[20] R.G. Littlejohn, J. Math. Phys. 20 (1979) 2445;
R.G. Littlejohn, Phys. Fluids 24 (1981) 1730;
R.G. Littlejohn, J. Plasma Phys. 29 (1983) 111.
[21] B.B. Kadomitsev, O.P. Pogutse, Reviews of Plasma Physics, Turbulence in Toroidal Systems, vol. 5, Consultants Bureau, New York, 1970 (Chapter 2).
[22] A.B. Mikhailovskii, Theory of Plasma Instabilities, vol. 2: Instabilities of an Inhomogeneous Plasma, Consultants Bureau, New York, 1974.
[23] W.M. Tang, Nucl. Fusion 18 (1978) 1089.
[24] W. Horton, Rev. Mod. Phys. 71 (1999) 735.
[25] S.I. Braginskii, in: M.A. Leontovich (Ed.), Reviews of Plasma Physics, vol. I, Consultants Bureau, New York, 1965, p. 205.
[26] G.W. Hammett, F.W. Perkins, Phys. Rev. Lett. 64 (1990) 3019.
[27] N. Mattor, S.E. Parker, Phys. Rev. Lett. 79 (1997) 3419.
[28] H. Sugama, et al., Phys. Plasmas 8 (2001) 2617.
[29] R.E. Waltz, et al., Phys. Fluids B 4 (1992) 3138.
[30] W. Dorland, G.W. Hammett, Phys. Fluids B 5 (1993) 812.
[31] M.A. Beer, G.W. Hammett, Phys. Plasmas 3 (1996) 4018;
M.A. Beer, G.W. Hammett, Phys. Plasmas 3 (1996) 4046.
[32] M. Kotschenreuther, et al., Phys. Plasmas 2 (1995) 2381.
[33] R.E. Waltz, et al., Phys. Plasmas 4 (1997) 4046.
[34] M.N. Rosenbluth, F.L. Hinton, Phys. Rev. Lett. 80 (1998) 724.
[35] M. Beer, G. Hammet, in: Proceedings of Varenna-Lausanne International Workshop, Societa Italiana di Fisica, Editrice Compositori, Bologna, 1998.
[36] C.K. Birdsall, A.B. Langdon, Plasma Physics via Computer Simulation, Adam Hilger, Bristol and New York, 1991.
[37] R.W. Hockney, J.W. Eastwood, Computer Simulation Using Particles, Adam Hilger, Bristol and New York, 1988.
[38] T. Tajima, Computational Plasma Physics: With Applications to Fusion and Astrophysics, Addison–Wesley, Redwood City, CA, 1989.
[39] W.W. Lee, Phys. Fluids 72 (1987) 243;
W.W. Lee, J. Comput. Phys. 72 (1987) 243.
[40] S.E. Parker, W.W. Lee, Phys. Fluids B 5 (1993) 77.
[41] A.Y. Aydemir, Phys. Plasmas 1 (1994) 822.
[42] S.J. Allfrey, R. Hatzky, Comput. Phys. Commun. 154 (2003) 98.
[43] R. Hatzky, et al., Phys. Plasmas 9 (2002) 898.
[44] S. Brunner, E. Valeo, J.K. Krommes, Phys. Plasmas 6 (1999) 4504.
[45] W.X. Wang, et al., Plasma Phys. Control. Fusion 41 (1999) 1091.
[46] G. Hu, J.A. Krommes, Phys. Plasmas 1 (1994) 863.
[47] Z. Lin, et al., Phys. Rev. Lett. 88 (2002) 195004;
Z. Lin, T.S. Hahm, Plasmas 11 (2004) 1099.
[48] M.J. LeBrun, et al., Phys. Fluids B 5 (1993) 752.
[49] Y. Kishimoto, et al., in: Proceedings of the 15th International Conference on Plasma Physics and Controlled Nuclear Fusion Research, IAEA, Vienna, 1994.
[50] G. Furnish, et al., Phys. Plasmas 6 (1999) 1227.
[51] S.E. Parker, W.W. Lee, R.A. Santoro, Phys. Rev. Lett. 71 (1993) 2042.

[52] R.D. Sydora, V.K. Decyk, J.M. Dawson, Plasma Phys. Control. Fusion 38 (1996) A281.
[53] A.M. Dimits, et al., Phys. Rev. Lett. 77 (1996) 71.
[54] Z. Lin, et al., Science 281 (1998) 1835.
[55] Y. Idomura, S. Tokuda, Y. Kishimoto, Nucl. Fusion 43 (2003) 234.
[56] Y. Chen, S.E. Parker, J. Comput. Phys. 189 (2003) 463.
[57] H. Naitou, et al., Phys. Plasmas 2 (1995) 4257.
[58] W.W. Lee, et al., Phys. Plasmas 8 (2001) 4435.
[59] Z. Lin, L. Chen, Phys. Plasmas 8 (2001) 1447.
[60] A. Mishchenko, R. Hatzky, A. Könies, Phys. Plasmas 11 (2004) 5480.
[61] C.Z. Cheng, G.K. Knorr, J. Comput. Phys. 22 (1976) 330.
[62] E. Sonnendrücker, et al., J. Comput. Phys. 149 (1999) 201.
[63] M. Brunetti, et al., Comput. Phys. Commun. 163 (2004) 1.
[64] Y. Sarazin, et al., in: Proceedings of the 20th IAEA Fusion Energy Conference, IAEA, Vienna, 2004.
[65] W. Dorland, et al., in: Proceedings of the 18th IAEA Fusion Energy Conference, IAEA, Vienna, 2000.
[66] F. Jenko, Comput. Phys. Commun. 125 (2000) 196.
[67] J. Candy, R. Waltz, J. Comput. Phys. 186 (2003) 545.
[68] T.H. Watanabe, H. Sugama, Nucl. Fusion 46 (2006) 24.
[69] R.D. Hazeltine, J.D. Meiss, Plasma Confinement, Addison–Wesley, Redwood City, CA, 1992.
[70] M.A. Beer, S.C. Cowley, G.W. Hammett, Phys. Plasmas 2 (1995) 2687.
[71] W.W. Lee, W.M. Tang, Phys. Fluids 31 (1988) 612.
[72] J.A. Krommes, G. Hu, Phys. Plasmas 1 (1994) 3211.
[73] H. Sugama, et al., Phys. Plasmas 3 (1996) 2379.
[74] T.-H. Watanabe, H. Sugama, T. Sato, J. Phys. Soc. Japan 70 (2001) 3565.
[75] T.-H. Watanabe, H. Sugama, Phys. Plasmas 9 (2002) 3659.
[76] T.-H. Watanabe, H. Sugama, Phys. Plasmas 11 (2004) 1476.
[77] G.K. Batchelor, Fluid Mech. 5 (1959) 113.
[78] K.H. Burrell, Phys. Plasmas 4 (1997) 1499.
[79] P.W. Terry, Rev. Mod. Phys. 72 (2000) 109.
[80] X. Garbet, Plasma Phys. Control. Fusion 43 (2001) A251.
[81] T.S. Hahm, Plasma Phys. Control. Fusion 44 (2002) A87.
[82] J.W. Connor, et al., Nucl. Fusion 44 (2004) R1.
[83] H. Biglari, P.H. Diamond, P.W. Terry, Phys. Fluids B 2 (1990) 1.
[84] T.S. Hahm, K.H. Burrell, Phys. Plasmas 2 (1995) 1648.
[85] R.E. Waltz, et al., Phys. Plasmas 1 (1994) 2229.
[86] T.S. Hahm, et al., Phys. Plasmas 6 (1999) 922.
[87] S.J. Allfrey, et al., New J. Phys. 4 (2002) 29.
[88] R.E. Waltz, J. Candy, M.N. Rosenbluth, Phys. Plasmas 9 (2002) 1938.
[89] A. Hasegawa, Adv. Phys. 34 (1985) 1.
[90] W. Horton, A. Hasegawa, Chaos 4 (1994) 227.
[91] V. Naulin, New J. Phys. 4 (2002) 28.1.
[92] A. Hasegawa, K. Mima, Phys. Fluids 21 (1978) 87.
[93] J.G. Charney, Geofys. Publ. 17 (1948) 3.
[94] A. Hasegawa, Y. Kodama, Phys. Rev. Lett. 41 (1978) 1470.
[95] P.B. Rhines, J. Fluid. Mech. 69 (1975) 417.
[96] P.H. Diamond, et al., Nucl. Fusion 41 (2001) 1067.
[97] L. Chen, Z. Lin, R. White, Phys. Plasmas 7 (2000) 3129.
[98] P.H. Diamond, et al., in: Proceedings of the 17th IAEA Fusion Energy Conference, IAEA, Vienna, 1998.
[99] B.N. Rogers, W. Dorland, M. Kotschenreuther, Phys. Rev. Lett. 85 (2000) 5336.
[100] J. Li, Y. Kishimoto, Phys. Plasmas 9 (2002) 1241.
[101] F. Jenko, W. Dorland, Phys. Rev. Lett. 89 (2002) 225001.
[102] Y. Idomura, M. Wakatani, S. Tokuda, Phys. Plasmas 7 (2000) 3551.
[103] E.J. Kim, P.H. Diamond, Phys. Plasmas 9 (2002) 4530.
[104] J. Li, Y. Kishimoto, Phys. Plasmas 11 (2004) 1493.
[105] Z. Lin, et al., Phys. Plasmas 7 (2000) 1857.
[106] F. Jenko, T. Dannert, C. Angioni, Plasma Phys. Control. Fusion 47 (2005) B195.
[107] Z. Lin, et al., Phys. Rev. Lett. 83 (1999) 3645.
[108] G.L. Falchetto, M. Ottaviani, Phys. Rev. Lett. 92 (2004) 25002.
[109] L. Villard, et al., Nucl. Fusion 44 (2004) 172.
[110] G.R. McKee, et al., Nucl. Fusion 41 (2001) 1235.
[111] H. Shirai, et al., J. Phys. Soc. Japan 64 (1995) 4209.
[112] R.V. Budny, et al., Phys. Plasmas 7 (2000) 5038.
[113] S.E. Parker, C. Kim, Y. Chen, Phys. Plasmas 6 (1999) 1709.

[114] J. Candy, R.E. Waltz, Phys. Rev. Lett. 91 (2003) 45001;
R.E. Waltz, et al., Nucl. Fusion 45 (2005) 741.
[115] J.W. Connor, J.B. Taylor, H.R. Wilson, Phys. Rev. Lett. 70 (1993) 1803.
[116] F. Romanelli, F. Zonca, Phys. Fluids B 5 (1993) 4081.
[117] J.Y. Kim, M. Wakatani, Phys. Rev. Lett. 73 (1994) 2200.
[118] X. Garbet, R.E. Waltz, Phys. Plasmas 3 (1996) 1898.
[119] X. Garbet, Nucl. Fusion 34 (1994) 963.
[120] L. Chen, R.B. White, F. Zonca, Phys. Rev. Lett. 92 (2004) 75004.
[121] J. Candy, R.E. Waltz, W. Dorland, Phys. Plasmas 11 (2004) L25.
[122] G. Rewoldt, W.M. Tang, M.S. Chance, Phys. Fluids 25 (1982) 480.
[123] J.Y. Kim, W. Horton, J.Q. Dong, Phys. Fluids B 5 (1993) 4030.
[124] G. Rewoldt, W.M. Tang, Phys. Fluids B 2 (1990) 318.
[125] S.E. Parker, et al., Phys. Plasmas 11 (2004) 2594.
[126] J. Candy, Phys. Plasmas 12 (2005) 72307.
[127] D.R. Ernst, et al., Phys. Plasmas 11 (2004) 2637.
[128] T. Dannert, F. Jenko, Phys. Plasmas 12 (2005) 72309.
[129] K. Hallatscheck, W. Dorland, Phys. Rev. Lett. 95 (2005) 55002.
[130] Y. Idomura, S. Tokuda, Y. Kishimoto, Nucl. Fusion 45 (2005) 1571.
[131] W. Dorland, et al., Phys. Rev. Lett. 85 (2000) 5579.
[132] Z. Lin, L. Chen, F. Zonca, Phys. Plasmas 12 (2005) 56125.